Environmental Science & Technology

Article

Cite This: Environ. Sci. Technol. 2018, 52, 4051−4060

pubs.acs.org/est

Membrane Capacitive Deionization with Constant Current vs Constant Voltage Charging: Which Is Better?

Li Wang[†] and Shihong Lin*[,†,‡]

[†]Department of Civil and Environmental Engineering, Vanderbilt University, Nashville, Tennessee 37235-1831, United States

[‡]Department of Chemical and Biomolecular Engineering, Vanderbilt University, Nashville, Tennessee 37235-1831, United States

Supporting Information

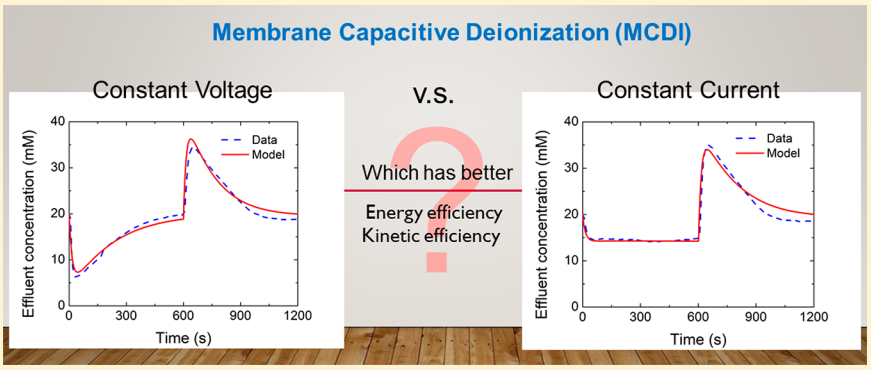

ABSTRACT: Membrane capacitive deionization (MCDI) can be typically operated with constant voltage (CV) or constant current (CC) mode in the charging stage. While a series of previous studies have compared both charging modes to identify the better operating mode, neither their performance evaluation protocols were consistent, nor did their conclusions unanimously converge. This study presents a new framework to evaluate and compare MCDI performance, considering the kinetic efficiency, the energetic efficiency, and the intrinsic trade-off between the two. A key prerequisite for making rational comparison of performance between MCDI operations is that the operations being compared should all result in the same target adsorption. With this key prerequisite and the new evaluation framework based on the trade-off curve between kinetic and energetic efficiencies, our experimental assessment and theoretical analysis suggest that whether CC or CV charging is more efficient is strongly dependent on the target adsorption and, to a less extent, on the kinetic rate of charging. However, the advantage in energy or kinetic efficiency of one charging mode over that of the other is relatively small in all cases. Our study also reveals that, for a given MCDI system, there exist regimes of target adsorptions and kinetic rates that can only be achieved by either CC or CV charging, or even regimes that can be achieved by neither charging mode. In summary, this study revises our current understanding regarding the comparison of the two typical charging modes in MCDI, and introduces a new framework for comparing the performance of different MCDI and CDI operations.

INTRODUCTION

Capacitive deionization (CDI) is an emerging technology for water desalination by the means of adsorbing ions in charged electrodes.[1] Compared to existing desalination technologies such as thermal distillation and reverse osmosis, CDI has several technological features, including the capability of desalinating low-to-moderate salinity feedwater with low energy consumption,[2,3] flexibly tailorable effluent salinity,[4] and the compatibility with intermittent operation.[5] These advantages render CDI a promising technology for desalinating brackish water with low-to-moderate feed salinity, especially in the context of off-grid and on-demand desalination powered by renewable energy.[6,7]

Over the past decades, CDI has received extensive academic and industrial interest and experienced a significant growth in research and development. Advances have been made in multiple aspects, including developing high-performance electrodes,[8−12] modeling dynamic ion transport in CDI electrodes,[13−16] designing novel cell stack structures that enhance performance or enable continuous operation,[5,17−20] and elucidating the impacts of the operating modes and electrode properties on CDI performance.[4,21−26] Of these technological advancements, membrane CDI, or MCDI, that is, CDI coupled with ion exchange membranes (IEMs), received particular attention due to its higher charge efficiency and better energy efficiency.[14,27]

The two most common charging modes in CDI/MCDI are constant voltage (CV) and constant current (CC).[1] In CV charging, a constant voltage is applied across the CDI/MCDI cell throughout the charging stage. The electrical current through the cell and the kinetic rate for ion removal spike immediately after

Received: November 24, 2017
Revised: February 26, 2018
Accepted: March 12, 2018
Published: March 12, 2018

DOI: 10.1021/acs.est.7b06064
Environ. Sci. Technol. 2018, 52, 4051−4060

charging starts, and then decrease as the electrodes become increasingly saturated with the adsorbed ions. In CC charging, the cell voltage is automatically increased to maintain a constant current during the charging stage. Since the ion transfer kinetic rate is roughly proportional to the charging current, ions are also removed in a constant rate during CC charging.

Both CC and CV charging have been heavily studied and proven viable in CDI/MCDI. Several previous studies compared CDI/MCDI performance with the two charging modes, the results of which are summarized in Table 1. With only one exception, all studies suggest that CC charging consumes less energy than CV charging to remove the same amount of salt, and is thus a more energy efficient charging mode. In addition, one study found that MCDI with CV operation adsorbs more salt per charging stage than that with CC operation when the charging voltage in CV equals the final charging voltage in CC.[28,29] Interestingly, however, the study by Zhao et.al. suggested that there exist subtle differences between the energy consumption with CC and CV charging, and that such differences depend on the charging time, the feed salinity, and the levels of the applied voltage in CV operation and current in CC operation.[4] It is worth noting that the experimental protocols of these studies are all different, thus the interpretation of the conclusions in Table 1 has to be practiced with caution regarding their specific experimental protocols.

Table 1. Summary of Previous Studies That Compared CC and CV Operations

CDI type[a]	experimental protocol	conclusions	ref
MCDI	• CV charging voltage equals CC cutoff voltage (0.4 to 1.4 V) • CC with fixed current density • identical charging time	• CC more energy efficient • CV adsorbs more salt	28
CDI	• CV charging voltage and CC cutoff voltage both @ 1.2 V • CC with different current densities • equal total charge transferred or total amount of salt adsorbed	• CC more energy efficient	29
CDI	• CV charging voltage equals CC cutoff voltage (1.2 V)	• CC more energy efficient	30
flow-through CDI	• CV charging voltage @ 1 V with different charging time • equal total charge transferred • identical charging time	• CC more energy efficient	31
MCDI and CDI	• CV charging voltage @ 1.2 V with a charging time of 300 s • CC charging current @ 1.0 A[b] and cutoff voltage @ 1.6 V • various feed salinity	• MCDI more energy efficient than CDI • no conclusive advantage in energy efficiency for CC or CV	4

[a]All CDI or MCDI processes are of flow-by configuration unless specified otherwise. [b]The corresponding current density was 38.4 A m^{-2}.

Answering the question of whether CC or CV is a better charging mode for MCDI requires the definition of "better". From a practical operation perspective, a better charging is one that either consumes less energy at the same ion removal rate, or removes ions faster with the same energy consumption, or even consumes less energy and removes ion faster. This performance evaluation metric composed of the energetic and kinetic efficiencies can be directly employed to evaluate the capital cost, which is related to the footprint and material cost of the system, and the operating cost, which is strongly dependent on the energy cost of desalination.[32,33] In this sense, the widely investigated parameter, specific adsorption capacity (SAC) in the charging stage, is only of indirect significance that would ultimately be integrated to the kinetic and/or energetic efficiencies.

Following the rationale above, a performance evaluation framework has been recently developed to quantify the trade-off between energetic and kinetic efficiencies using trade-off curves that relate the inverse of specific energy consumption, SEC^{-1} (i.e., amount of salt per unit energy consumed), and the average salt adsorption rate, ASAR (i.e., amount of salt adsorbed per mass of electrode per time).[33] Increasing the ASAR, which quantifies the kinetic efficiency, along the "SEC^{-1} vs ASAR" trade-off curve, reduces the SEC^{-1}, which reflects the energetic efficiency. Each point on a "SEC^{-1} vs ASAR" trade-off curve represents a charging operation defined by the selection of three parameters, including the applied voltage in a CV operation or the applied current in a CC operation, the flow rate of the flow stream through the system, and the duration of the charging stage. These parameters are carefully adjusted so that all points on a "SEC^{-1} vs ASAR" trade-off curve correspond to an identical "target adsorption". Different charging operations are considered to achieve the same "target adsorption" if the dilute solution volume, v_D, the initial salinity, c_0, and the average dilute solution salinity, $\overline{c}_D$, are maintained the same in these operations. It is of critical importance to ensure that all points on one "SEC^{-1} vs ASAR" trade-off curve result in the same target adsorption because different target adsorptions intrinsically, regardless of how they are achieved, require different minimum energy to charge the electrode to an end state characterized by the final voltage and charge density.[34]

Similarly, a rational comparison between CC and CV charging also requires that the two operations compared achieve the same target adsorption defined by v_D, c_0, and $\overline{c}_D$. Most previous studies comparing CC and CV charging did not make the deliberate effort to ensure the target adsorptions that the two operations achieve were identical, except for a recent study in which the charging duration and total transferred charge for both CC and CV charging were maintained the same.[31] To compare the two charging modes systematically, two series of experiments can be conducted to construct two "SEC^{-1} vs. ASAR" trade-off curves, one for CC charging and the other for CV charging, both resulting in an identical target adsorption. Theoretically, the intersection between two trade-off curves implies the existence of an ASAR above which one charging mode is better and below which the other charging mode outperforms. Otherwise, one can conclude that a charging mode is consistently superior to the other, at least for achieving a specific target adsorption. This is the theoretical framework we will employ to systematically compare CC and CV charging in MCDI.

In this study, we employ both experimental and simulation approaches to investigate the kinetic and energetic efficiencies of MCDI with CV and CC charging. The performance comparison between these two charging modes is carried out by comparing the relative positions of their trade-off curves that relate the kinetic and energetic efficiencies of a series of operations resulting in the same target adsorption. We also evaluate the equilibrium voltage and excess voltage over a charging stage, from which we calculate the excess energy to elucidate why one charging mode outperforms the other. We focus our comparison on the charging (or adsorption) stage in this study, instead of the

DOI: 10.1021/acs.est.7b06064
Environ. Sci. Technol. 2018, 52, 4051−4060

full charging-discharge MCDI cycle, because the flexibility of choosing different discharge modes and kinetic rates for a given charging stage complicates the comparison of a full cycle and renders the analysis more arbitrary and less insightful. Our primary goal is to determine if there exists one charging mode that universally outperforms another, and if not, to identify factors affecting their relative performance.

MATERIALS AND METHODS

MCDI Stack. The MCDI stack design has been described in our previous publication and its details are given in the Supporting Information.[33] Briefly, four electrodes/membranes/spacer assemblies were firmly compacted into a MCDI stack in an acrylic housing. Each assembly consisted of two porous carbon electrodes (PACMM 203, Materials & Methods LLC, Irvine, CA) with a thickness of δ_e = 280 μm, an anion exchange membrane (Neosepta AMX, Tokuyama Co., Japan) with a thickness of δ_{amem} = 140 μm, a cation exchange membrane (Neosepta CMX, Tokuyama Co., Japan) with a thickness of δ_{cmem} = 170 μm, and a glass fiber spacer (Whatman) with a thickness of δ_{sp} = 250 μm. Each assembly was cut into a 6 × 6 cm^2 square with a 1.5 × 1.5 cm^2 square hole at the center. The total mass of the four pairs of electrodes was 3.06 g. The feed solution enters from the periphery of the stack, flows along the spacer channels, and exits through the square cutout in the center.

Experimental Methods. In all experiments, the feed solution was a 20 mM NaCl solution. The feed reservoir was constantly purged with nitrogen to remove dissolved oxygen for minimizing long-term electrode oxidation. The feed solution was peristaltically pumped through the MCDI stack, and the effluent of the MCDI stack was sent back to the feed reservoir. The effluent conductivity was measured using an inline conductivity meter (isoPod EP357, eDAQ, Australia) installed right at the exit of the MCDI cell, and was further converted to salt concentration based on a pre-established calibration curve. Both CV and CC charging modes were applied using a potentiostat (SP 150, Bio-Logic, France) that also measured the real-time electrical current in the CV mode and the real-time cell voltage in the CC mode.

Identical Target Adsorption and Kinetic Rate. Following the rationale presented in the introduction, the fair comparison of the performance between two CDI/MCDI systems, either with different electrode materials, configurations, or operation modes, entails that the two operations achieve identical target adsorption at the same kinetic rate. This rationale was implemented throughout this study for comparing CC and CV charging. Specifically, we carefully adjusted the experimental conditions to make sure that the *average dilute solution salinity*, $\overline{c}_D$, and the *dilute solution volume*, v_D, were kept constant in MCDI experiments with both CC and CV charging. (c_0 was also constant in all cases). To achieve identical target adsorption with both CC and CV modes, we first run MCDI experiments with CV charging to obtain $\overline{c}_D$, and then adjusted the current in CC charging to achieve a mean effluent concentration that is equal to the $\overline{c}_D$ in CV charging. The first series of experiments in this study were conducted to achieve a $\overline{c}_D$ of 14.4 mM (from c_0 = 20 mM), for a dilute solution volume of v_D = 100 mL. Other target adsorptions were also investigated, with their detailed parameters given in discussion. The operating parameters for the experiments, including flow rate and charging duration, applied voltage in CV charging, and applied current in CC charging are all reported in Table S1. The MCDI cell was operated for several cycles to allow the electrode to reach dynamic adsorption−desorption equilibrium. All charge/discharge cycles selected for data analysis were chosen from a series of at least three consecutive full cycles that yield very similar time series of effluent salinity. The actual $\overline{c}_D$ with different experimental conditions, which are supposed to be around 14.4 mM, are reported in Table S2.

In addition to identical target adsorption, another requirement for direct comparison of the energy efficiency between two charging modes is that they remove salts at the same kinetic rate, which is typically quantified by ASAR. Because the total amount of salt removed in the adsorption stage is $(c_0 - \overline{c}_D)v_D$, and also because $\overline{c}_D$ and v_D are both controlled to be the same for achieving identical target adsorption, the total amount of salt removed in the adsorption stage is the same for the two charging modes. Therefore, an equal ASAR also requires that the same charging duration and cross flow rate are maintained for both CC and CV charging. The detailed conditions for different sets of experiments are summarized in Table S1.

Data Analysis. For CV charging, the effluent salinity, c_D, varies over the entire charging stage. Even for CC operation in which c_D is supposed to be constant, c_D also varies briefly at the beginning of the charging stage before becoming stable, because the effluent exiting the cell right after the charging starts is exposed to the applied electric field for a duration less than hydraulic contact time. Because of the temporal variability of c_D, the average effluent salinity for an MCDI charging stage, $\overline{c}_D$, is estimated for each adsorption mode using eq 1:

$$\overline{c}_D = \frac{\int_0^{t_C} c_D(t)\,\mathrm{d}t}{t_C} \tag{1}$$

where $c_D(t)$ is the real-time effluent salinity and t_C is the time of the charging duration.

The energy efficiency of an MCDI process has been traditionally quantified using specific energy consumption, SEC, defined as the energy consumed to remove a unit mole of NaCl:

$$\mathrm{SEC} = \frac{\int_0^{t_C} I(t)\,V(t)\,\mathrm{d}t}{Q\int_0^{t_C}(c_0 - c_D(t))\,\mathrm{d}t} \tag{2}$$

where $I(t)$ is the electrical current, $V(t)$ is the cell voltage, Q is the flow rate, and c_0 is the feed concentration. Alternatively, we can also quantify energy efficiency of an MCDI process using the inverse of SEC, that is, SEC^{-1}. SEC^{-1}, being the mass of salt removed with a unit energy input, directly reflects how efficiently energy is utilized for salt removal. Notably, SEC^{-1} is essentially the same as energy-normalized adsorbed salt (ENAS) that was used in a previous study.[35] We use SEC^{-1} instead of SEC to present our data in this study because the negative correlation between SEC^{-1} and kinetic rate of salt removal better reflects the intrinsic trade-off between energetic and kinetic efficiencies.

Finally, the kinetic efficiency of an MCDI process is quantified by ASAR which can be evaluated using eq 3:

$$\mathrm{ASAR} = \frac{Q\int_0^{t_C}(c_0 - c_D(t))\,\mathrm{d}t}{\theta_e t_C} \tag{3}$$

where θ_e represents either the mass or the apparent area of the electrode. While the definition of ASAR based on electrode mass is most commonly used in literature, defining ASAR based on apparent area of electrode and IEM assembly may be more informative in practical system design because it better reflects

DOI: 10.1021/acs.est.7b06064
Environ. Sci. Technol. 2018, 52, 4051−4060

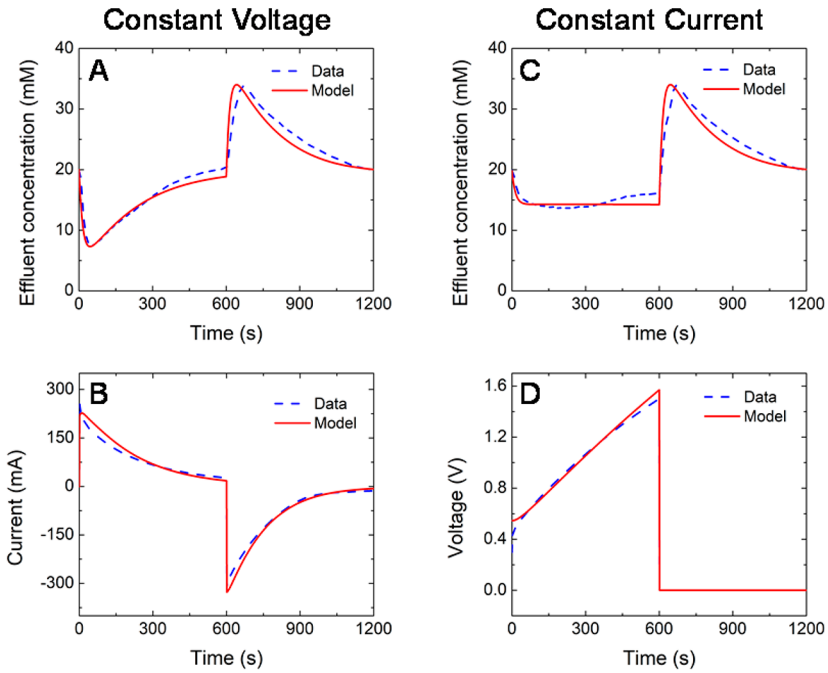

Figure 1. (A) Effluent concentration and (B) electrical current in an MCDI process with CV charging; (C) effluent concentration and (D) cell voltage in an MCDI process with CC charging. The charging voltage for the CV operation was 1.2 V. The electrical current in the CC operation was 92 mA. In both cases, the discharge was carried out using zero voltage. The target adsorption is quantified by a c_0 of 20 mM, a $\overline{c}_D$ of 14.4 mM, and a v_D of 100 mL.

the demand for both electrode and IEM. Therefore, both definitions of ASAR will be reported in this study. We also note that ASAR in the following discussion is defined based on the charging time, not the full cycle time, unless specified.

The comparison between two MCDI charging operations can be performed by simultaneously comparing their SEC^{-1} and ASAR, provided that they achieve the same target adsorption. For example, if two charging operations are of the same SEC^{-1}, i.e., they are equally energy efficient, the one with a higher ASAR, i.e., the one that removes salt faster, can be considered more kinetically efficient and thus "better". Similarly, if two operations are of the same ASAR, the one with a higher SEC^{-1} is considered to be "better" because it is more energy efficient. If the"SEC^{-1} vs ASAR" trade-off curve of one charging mode is completely above that of the other charging mode throughout the range of ASAR they overlap, we can conclude the charging mode with a higher trade-off curve to be more efficient in general.

■ DYNAMIC ION TRANSPORT MODEL

We employed a dynamic ion transport model to extract parameters of our MCDI system by fitting experimental data and used such a model to conduct more comprehensive theoretical analysis comparing CC and CV charging over a larger range of operating conditions. This model considers ion transport across ion exchange membranes (IEMs) and within the macropores of the carbon electrodes, as well as the equilibrium ion distribution at the interfaces between the spacer and IEMs, between IEMs and macropores of the carbon electrode, and between micropores and macropores of the carbon electrodes.[14,36] The porous carbon electrodes are assumed to be inherently charge-free and are charged only when a nonzero external voltage is applied.[34,37]

With an applied external voltage, a Donnan potential is established between the micropores and macropores according to the modified Donnan (mD) model.[14] Similarly, Donnan potentials also exist at the IEMs/spacer and IEMs/electrode interfaces.[38] Additional potential drops across an MCDI half-cell include the Stern potential between the electronic and ionic charges, potential drops due to ion transport resistance in the IEMs and spacer, electronic resistance in the carbon electrodes, and contact resistances at various interfaces (primarily at the electrode/current collector interfaces[39]). These parasitic potential drops, together with the Donnan and Stern potentials, comprise the cell voltage. In the direction of the water flow along the spacer channel, the MCDI cell is modeled as a continuous stirred-tank reactor (CSTR), that is, we do not consider the concentration gradient in the flow direction.[40] This dynamic MCDI ion transport model was numerically solved to predict the time-dependent effluent salinity and the cell current (in CV charging) or cell voltage (in CC charging), which were then compared with experimental results and to generate performance parameters such as ASAR and SEC^{-1}. The details of the model derivation and the parameter selection are provided in the Supporting Information.

■ RESULTS AND DISCUSSION

Experimental Results and Model Validation. In the first series, five pairs of MCDI experiments were conducted for performance comparison between CV and CC charging. Each pair comprises one MCDI experiment with CV charging and the other with CC charging, respectively. All five pairs of MCDI experiments achieved a very similar target adsorption, characterized by a c_0 of 20 mM, a $\overline{c}_D$ of 14.4 mM, and a v_D of 100 mL. Figure 1 presents the experimental and modeling results for one pair of experiments in which the applied voltage in CV operation was 1.2 V and the electrical current in CC operation was 92 mA. The flow rate for both operations was 10 mL min^{-1}. For both CV (Figure 1A and 1B) and CC (Figure 1C and 1D) charging, a dynamic MCDI model with an identical set of parameters (Table S3) fits the experimental results remarkably well. The same set of

DOI: 10.1021/acs.est.7b06064
Environ. Sci. Technol. 2018, 52, 4051−4060

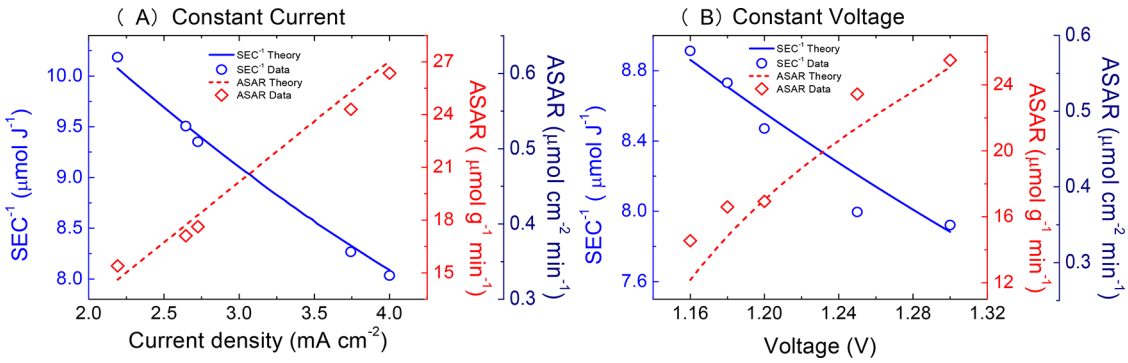

Figure 2. SEC^{-1} (blue, left *y*-axis) and ASAR (right, *y*-axis) for charging stage as functions of current density in CC mode (A) and cell voltage in CV mode (B). The open circles and diamonds are experimental data, whereas the dash and solid curves (lines) are results simulated from the dynamic ion transport model with a single set of parameters listed in Table S3. The target adsorption is quantified by c_0 of 20 mM, a $\overline{c}_D$ of 14.4 mM, and a ν_D of 100 mL.

parameters, which are theoretically dependent only on the properties of the MCDI system but not on the operating conditions, will be applied for MCDI modeling in the rest of this work.

In addition to the excellent agreement between experimental and modeling results, the time dependent profiles of effluent salinity, electrical current (in CV charging), and cell voltage (in CC charging) are highly consistent with the state-of-the-art experimental results reported in the literature.[4,41] Results from Figure 1 also demonstrate the ability to control the operating conditions in CV and CC charging to achieve the same target adsorption at the same ASAR, which is the foundation for fair comparison of system performance between the two operation modes.

Additional MCDI experiments similar to those shown in Figure 1 were performed by varying the cell voltage in CV charging, the cell current in CC charging, the flow rate, and charging/discharging duration, all controlled to yield the same target adsorption. Their energy efficiency, quantified by SEC^{-1}, and kinetic efficiency, quantified by ASAR, varied as a function of the driving force, quantified by either the cell voltage or cell current (Figure 2). The ranges of cell voltage in CV operation (1.16 V to 1.30 V) and cell current in CC operation (74 mA to 135 mA) were chosen such that both operation modes yield a similar range of ASAR.

The simulated results from the dynamic ion transport model, given in Figure 2 as solid and dash curves, fit the experimental data reasonably well for both CV and CC chagrining. The good fitting, demonstrated by the high coefficients of determination (Table S5), suggests a remarkable predicting power of the MCDI ion transport model, especially given that these curves are not established by fitting the experimental data but rather completely simulated from the dynamic ion transport model using one single set of system parameters. For both charging modes, SEC^{-1} negatively correlates with the cell voltage or current, whereas the ASAR positively correlates with the cell voltage or current.

Comparing CC and CV Charging. The results in Figure 2 are used to construct the SEC^{-1} vs ASAR trade off curve that reflects the intrinsic trade-off between energetic and kinetic efficiencies in MCDI (Figure 3). These trade-off curves indicate that one can tune MCDI operation by increasing either the charging voltage in CV or the electrical current in CC charging to achieve a higher kinetic efficiency (ASAR) but at the cost of lower energy efficiency (SEC^{-1}), or in other words, higher energy consumption (SEC). We want to reemphasize that all

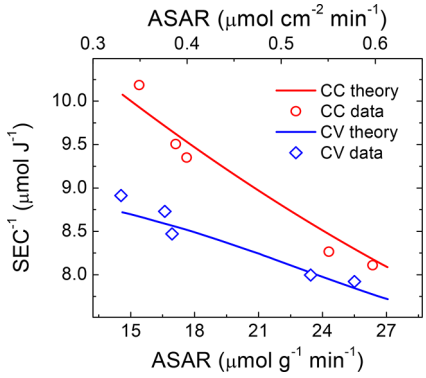

Figure 3. SEC^{-1} vs ASAR for the charging stage in MCDI with CC (red) and CV (blue) charging. These trade-off curves are constructed using the data shown on Figure 2. The open circles are experimental data, whereas the solid curves (lines) are results simulated from the dynamic ion transport model. Each data point on a CV trade-off curve is obtained with a unique cell voltage, as each point on a CC trade-off curve is obtained with a unique electrical current. The target adsorption is quantified by c_0 of 20 mM, a $\overline{c}_D$ of 14.4 mM, and a ν_D of 100 mL. The same SEC^{-1} vs ASAR curves with ASAR defined based on the full cycle time (i.e., including the time of zero voltage discharge) are reported in Figure S2. The change in ASAR definition does not change the relative position of the two curves.

experimental and simulated data points in Figure 3 result in the same target adsorption, which is critically important for comparison within and between the trade-off curves to be fully meaningful.

Comparing the two SEC^{-1} vs ASAR curves in Figure 3 suggests that CC charging is consistently better, by about 10 to 15%, than CV charging—at least for this specific target adsorption and within this range of kinetic rate. Such superiority can be interpreted from two different angles. First, if both CC and CV MCDI processes are operated at the same ASAR, CC charging is more energy efficient than CV charging as it removes more salt with the same amount of energy. Alternatively, if the MCDI process with the two charging modes are controlled to achieve equal energy efficiency, or SEC^{-1}, then CC charging removes salts appreciably faster than CV charging. Because the two trade-off curves do not intersect, we can conclude that CC charging is consistently more efficient than CV charging for this target adsorption and within this ASAR range.

Excess Voltage and Excess Energy. To elucidate why CC charging outperforms CV charging in the above example, here we

DOI: 10.1021/acs.est.7b06064
Environ. Sci. Technol. 2018, 52, 4051−4060

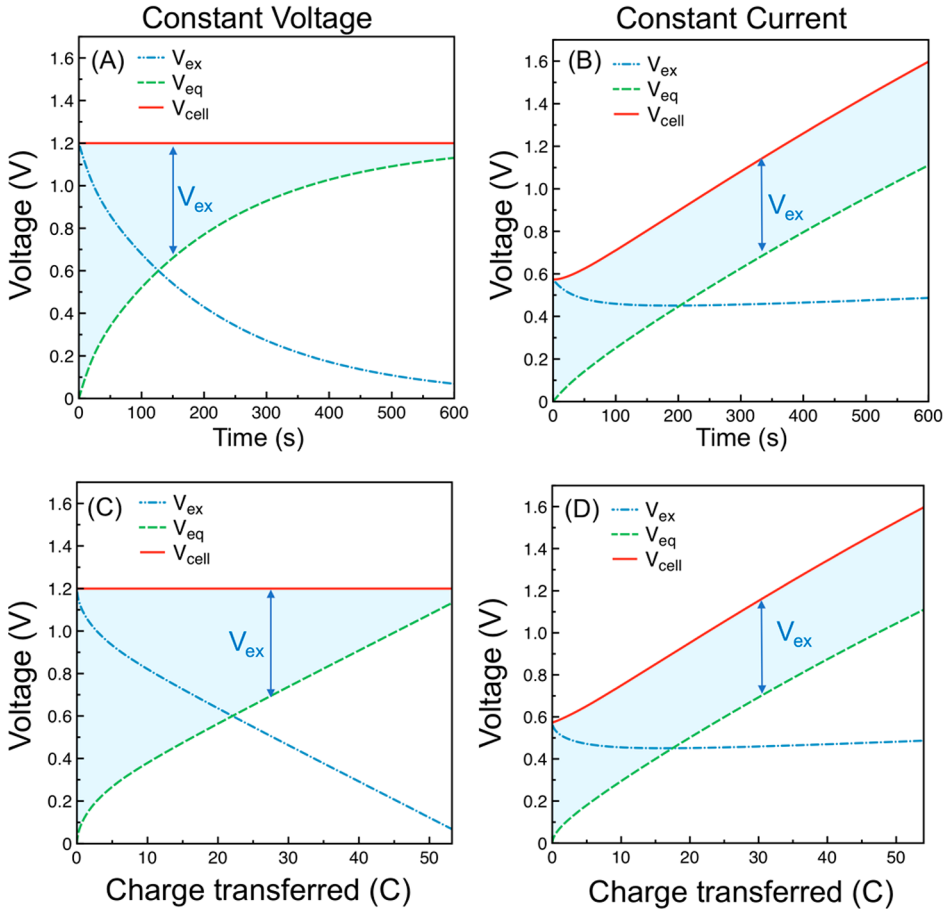

Figure 4. Distribution of cell voltage, V_{cell} (red solid curve), equilibrium voltage, V_{eq} (green dash curve), and excess voltage, V_{ex} (blue dash-dotted curve) over the charging stage. Panels A and B present the temporal distributions of these voltages in CV charging and CC charging, respectively. Panels C and D present the distribution of these voltages with respect to cumulative charge transferred in CV and CC charging, respectively. The excess voltage, V_{ex}, being the difference V_{cell} and V_{eq}, is also equal to the height of the shaded area. These figures are constructed using data presented in Figure 1 which were obtained from experiments in which the flow rate was 10 mL min^{-1}, charging time was 600 s, and the corresponding ASAR was about 17 μmol g^{-1} min^{-1}. Note that the total shaded area in panels C and D quantify the excess energy, that is, the total energy lost in the charging stage due to entropy generation.

introduce two important concepts: excess voltage and excess energy. Excess voltage, V_{ex}, is the difference between the actual cell voltage, V_{cell}, and the equilibrium cell voltage, V_{eq}:

$$V_{ex} = V_{cell} - V_{eq} \tag{4}$$

The equilibrium cell voltage is the imaginary cell voltage at which the system, with the ion distribution between the bulk solution and electrode micropores at a given moment, t, is in a thermodynamic equilibrium. In other words, if at any given point of a CDI/MCDI process, V_{cell} is adjusted to be equal to V_{eq}, the ion distribution at that point will be indefinitely maintained and no net ion transport into or out of the double layer in the micropores will occur. With a modified Donnan model,[34] V_{eq} is simply the sum of Donnan potentials, ΔV_D, Stern potentials, ΔV_{st}, and the Donan potentials across the two interfaces of IEMs (i.e., membrane/spacer and membrane/electrode interfaces). The equilibrium voltage is independent of any ion or electronic transport resistance, because these resistances are irrelevant without charge transport at a finite rate. Therefore, V_{ex} can be interpreted as the degree of deviation of the system from equilibrium, or as the driving force for ion transport. On the other hand, $V_{ex}(t)$ also equals the product of the electrical current, $I(t)$, and the total cell resistance, $R(t)$, at time, t. Therefore, the transient total system resistance $R(t)$ can be conveniently probed by evaluating $V_{ex}(t)$. However, resolving the different contributions to the total system resistance must be achieved using more complicated equivalent circuit models.[31]

The distribution of V_{ex} as a function of charging time in a CV operation differs drastically from that in a CC operation (Figure 4). In CC charging, V_{ex} is more evenly distributed throughout the charging stage, both temporally (Figure 4B) and per unit amount of charge transferred (Figure 4D). In contrary, V_{ex} in CV charging decreases over time from V_{cell} to approach zero, both temporally (Figure 4A) and per unit amount of charge transferred (Figure 4C). In CV charging, the "V_{ex} vs charge transferred" curve deviates significantly from the "V_{ex} vs. time" because the current was much higher at the beginning of charging. These two curves are of very similar shape in CC charging because the current is constant.

Another concept building on V_{ex} and more directly relevant to quantifying energy loss in a CDI or MCDI process is excess energy, E_{ex}, defined as the difference between the total energy consumed, E_{tot}, and the equilibrium energy, E_{eq}:

$$E_{ex} = E_{tot} - E_{eq} = \int_0^{\sigma_{e,t_c}} V_{cell}(\sigma_e)\, d\sigma_e - \int_0^{\sigma_{i,t_c}} V_{eq}(\sigma_i)\, d\sigma_i \tag{5}$$

where σ_e and σ_i are the cumulative electronic and ionic charges transferred, respectively, both being a function of time; σ_{e,t_c} and

DOI: 10.1021/acs.est.7b06064
Environ. Sci. Technol. 2018, 52, 4051−4060

σ_{i,t_c} are the cumulative electronic and ionic charges transferred at the end of the charging stage, t_c, respectively. Both σ_e and σ_i can be readily evaluated in real time. Specifically, $\sigma_e(t)$ is simply $\int_0^\tau I(\tau)\,d\tau$, and $\sigma_i(t)$ can be evaluated from the cumulative amount of salt removed at time t. For a charging process with a charge efficiency near unity, $\sigma_e(t)$ is close to $\sigma_i(t)$. When parasitic energy losses, such as from surface Faradaic reactions, do not contribute to ion removal, $\sigma_e(t)$ is larger than $\sigma_i(t)$.

The equilibrium energy, E_{eq}, represents the energy that is required to charge the MCDI cell to its final state of the charging half-cycle, if the charging is performed thermodynamically reversibly. We note E_{eq} comprises both capacitive energy stored in the carbon electrode and the potential energy associated with the Donnan potentials across the IEMs. On the basis of the definitions of σ_e, σ_i, and charge efficiency, $\eta(t)$, eq 5 can be rewritten as

$$E_{ex} = \int_0^{t_C} V_{cell}(t)\, I(t)\, (1 - \eta(t))\, dt - \int_0^{t_C} V_{ex}(t) I(t)\, \eta(t)\, dt \quad (6)$$

In an ideal scenario with η being unity, which is not a bad approximation for MCDI according to estimations summarized in Table S4, eq 6 can be further simplified to

$$E_{ex} = \int_0^{t_C} V_{ex}(t)\, I(t)\, dt = \int_0^{\sigma_{t_c}} V_{ex}(\sigma)\, d\sigma \quad (7)$$

where σ is σ_e or σ_i; and σ_{t_c} is σ_{e,t_c} or σ_{i,t_c}, because electron charge is always equal to ionic charge when the charge efficiency is one.

The analysis of E_{ex} and E_{eq} can provide additional important insights that are not reflected by assessing E_{tot} alone. Although we have shown in Figure 3 that CV charging consumes more energy than CC charging with the same average ASAR, it is theoretically possible CV charging does not dissipate more energy than CC charging but instead stores more energy that can potentially be recovered in the discharge half-cycle. The stored energy, which includes the capacitive contribution and the "salinity-gradient" contribution, theoretically differs between CC and CV charging even if the cumulative transferred charge is the same. This is because both contributions to the store energy depend on the final bulk concentration which is different in the two charging modes.

We analyze E_{ex} and E_{eq} of the MCDI charging half-cycles corresponding to the data points presented in Figure 3 and present their respective contributions to SEC in Figure 5. The comparison of SEC_{eq} between CC and CV charging suggests that the energy stored in these two charging processes is very similar, implying the relatively weak dependence of the stored energy on the bulk salinity at the end of the charging half-cycle. It becomes clear, by comparing SEC_{ex}, that the difference between SEC for CC and CV charging at the same ASAR is primarily attributable to the difference in the dissipated excess energy. Therefore, CC charging is indeed more efficient than CV charging for the specific target adsorption discussed so far, even after accounting for the energy stored in the two charging processes.

Can CV Charging Perform CC Charging? In all experimentally tested and numerically simulated scenarios in the above discussion, CC charging always outperforms CV charging, as reflected by the relative positions of their "SEC^{-1} vs ASAR" trade-off curves in Figure 3. This conclusion, however, is not universally true. We have conducted another series of experiments using both charging modes to achieve a different target adsorption characterized by the same feed and dilute solution concentrations (i.e., c_0 = 20 mM and $\overline{c}_D$ = 14.4 mM) but a different volume of dilute solution. Specifically, v_D in this new series of experiments was 50 mL, as compared to a v_D = 100 mL as in Figures 2, 3, and 5. The results from this second series of experiments suggest that CV charging is systematically more efficient than CC charging, as evidenced by an "SEC^{-1} vs ASAR" trade-off curve for CV charging that is consistently above that for CC charging (Figure 6A).

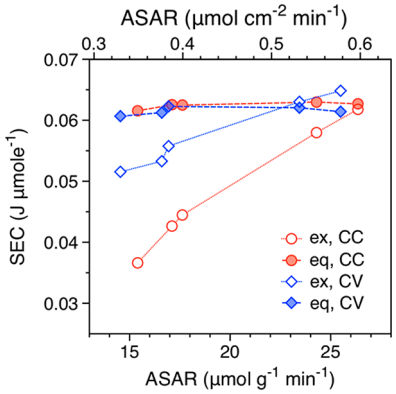

Figure 5. Comparison of excess SEC, SEC_{ex}, and equilibrium SEC, SEC_{eq} for CC and CV charging. SEC_{ex} and SEC_{eq} are calculated via normalizing E_{ex} and E_{eq} by the amount of salt adsorbed in the charging half-cycle (i.e., σ_{i,t_c}). These data are obtained by analyzing the charging half-cycles that yield the data on Figure 3. The target adsorption is quantified by a c_0 of 20 mM, a $\overline{c}_D$ of 14.4 mM, and a v_D of 100 mL. The dash and dotted lines are just a guide for the eyes.

Comparing SEC_{ex} and SEC_{eq} for adsorptions with a charging volume, v_D, of 100 mL (Figure 5) and those for adsorptions with a v_D of 50 mL (Figure 6B) leads to several observations. First, for a given v_D, SEC_{eq} is relatively independent of ASAR and charging mode. In addition, SEC_{eq} increases with increasing v_D, provided $\overline{c}_D$ is maintained the same; More interestingly, when v_D increases from 50 to 100 mL, SEC_{ex} increases for CV charging yet decreases for CC charging. Such changes are sufficiently significant to reverse the comparison of SEC_{ex} between the two operating modes. Specifically, CC charging dissipates more energy than CV charging with a v_D of 50 mL, but dissipates less energy than CV charging when v_D increases to 100 mL.

In addition to changing v_D, we also conducted an additional experiment to achieve a lower $\overline{c}_D$ of 10.4 mM for v_D = 50 mL. To achieve such an adsorption, the cell voltage in CV was set to 1.4 V and the charging process was terminated prematurely before the salt adsorption capacity of the electrodes was fully exhausted, as otherwise the high ASAR required was unattainable due to prolonged CV charging without adsorbing proportionally more salt. In this set of experiments (Figure S3), the ASAR for both charging modes was 31.7 μmol g^{-1} min^{-1}, whereas the SEC^{-1} for CV and CC charging were 7.87 and 7.19 μmol g^{-1} min^{-1}, respectively, suggesting that CV charging is 9.5% more energy efficient than CC charging at the same kinetic rate.

Relative Energetic-Kinetic Advantage Primarily Depends on the Target Adsorption. Up to this point, we have observed that CC and CV can both be the more efficient charging mode, and that their relative advantage in kinetic and energetic efficiencies is dependent on the target adsorption. For a more holistic comparison between CC and CV charging, we conduct additional simulations to cover a wider range of ASAR and target

DOI: 10.1021/acs.est.7b06064
Environ. Sci. Technol. 2018, 52, 4051−4060

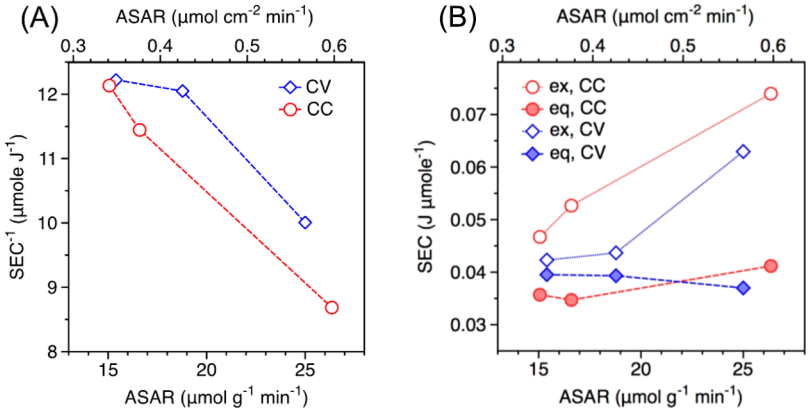

Figure 6. (A) SEC^{-1} vs ASAR for CV and CC charging. (B) SEC_{ex} and SEC_{eq} for CC and CV charging. The target adsorption is quantified by c_0 of 20 mM, a $\overline{c}_D$ of 14.4 mM, and a v_D of 50 mL. The dash and dotted lines are just a guide for the eyes.

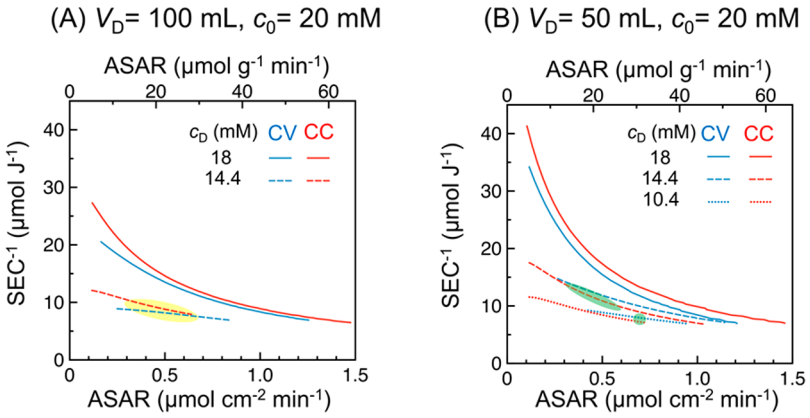

Figure 7. Simulated SEC^{-1} vs ASAR curves for CC (red) and CV (blue) charging with different "adsorptions" defined by different combinations of v_D, c_0, and $\overline{c}_D$. These results are simulated using the dynamic ion transport model described in the Supporting Information with parameters listed in Table S3. In all simulations, the feed salinity, c_0, is 20 mM. The dilute solution volumes, that is, the volumes of water passing through the MCDI stack in the adsorption stage, are 100 and 50 mL in panels A and B, respectively. The dilute solution salinity, c_D, varies within each subfigure. Each pair of CC and CV curves corresponds to one specific "adsorption". When simulating these data, we choose not to exceed 1.8 V for CC charging and 1.5 V for CV charging. These imposed constraints set the upper bounds of the ASARs for CV and CC charging. The lower bounds of the ASARs for CV charging result from the fact that CV charging with sufficiently low voltage to achieve ASARs below these lower bounds cannot provide enough salt adsorption capacity to achieve the target adsorption. Note that neither CV nor CC charging within the imposed voltage limits can possibly reduce the salinity of the 100 mL feed solution from 20 mM to 10.4 mM, which is why no curve is shown for such a target adsorption in panel A. The yellow region in panel A represents the data set presented in Figure 3, whereas the green region in panel B represents data set presented in Figure 6B. The green circle in panel B represents an additional data set reported in Supporting Information.

adsorptions using parameters in Table S3. The dynamic ion transport model can be considered reasonably reliable, as it yields predictions that are reasonably consistent with all experimental measurements. In all simulations, the feed salinity was c_0 = 20 mM. Two different dilute solution volumes, v_D = 100 mL and v_D = 50 mL, were evaluated. With each v_D, we tried to simulate the ASAR vs SEC^{-1} curves for CC and CV charging with $\overline{c}_D$ being 18 mM, 14.4 mM, and 10.4 mM, respectively.

Each trade-off curve for CC or CV charging has an upper limit of ASAR due to the maximum charging voltage chosen. The maximum ASAR in CC charging corresponds to an operation in which V_{cell} reaches a cutoff voltage of 1.8 V, whereas the maximum ASAR in CV charging corresponds to a maximum V_{cell} of 1.5 V. These operating voltage limits are set in our simulation because practical long-term operations beyond these limits will likely cause undesirable electrode oxidation.[42] The cutoff voltage for CC charging is chosen to be higher than the maximum applied voltage in CV charging, because electrodes are exposed to high voltage in CC charging for only a relatively short duration, whereas in CV charging the electrodes constantly experience the same voltage. In addition to these upper limits, there also exist lower limits of ASAR in CV charging. To achieve an ASAR below these limits, the MCDI cell has to operate at a voltage that is too low to adsorb enough salt for achieving the specified target adsorption (detailed explanation in Supporting Information).

For v_D = 100 mL (Figure 7A), CC charging is consistently more efficient than CV charging for target adsorptions that reduce $\overline{c}_D$ to 18 and 14.4 mM, which is reflected by the higher "SEC^{-1} vs ASAR" trade-off curves for CC charging than that for CV charging. When $\overline{c}_D$ is 14.4 mM, which is the target adsorption shown in Figure 2, the advantage of CC charging over CV charging diminishes with increasing ASAR as shown in Figure 3, but the two trade-off curves do not intersect within the chosen voltage limits for both charging modes. Neither CV nor CC charging can reduce $\overline{c}_D$ to 10.4 mM within their respective chosen voltage limits, because the salt adsorption capacities of the electrodes at those voltage limits are still lower than the amount of salt required to be removed to reach a $\overline{c}_D$ of 10.4 mM.

DOI: 10.1021/acs.est.7b06064
Environ. Sci. Technol. 2018, 52, 4051−4060

For target adsorptions with v_D = 50 mL (Figure 7B), whether one charging mode is more efficient than the other is highly dependent on $\overline{c}_D$. Specifically, CC charging is more efficient than CV charging throughout the range of possible ASAR when $\overline{c}_D$ is 18 mM. However, when $\overline{c}_D$ is 14.4 mM or 10.4 mM, CV charging becomes consistently better than CC charging, even though the advantage dwindles as ASAR decreases, which is consistent with Figure 6A.

The direct comparison between CC and CV charging is made only when both charging modes are able to attain the same target adsorptions at the same ASAR. There are, however, ranges of ASAR in which only one of the two charging modes can achieve the target adsorptions. Regardless of v_D, CC charging can operate at a wider range of ASARs than CV charging to achieve target adsorptions with a $\overline{c}_D$ of 18 mM. As a result, the ranges of ASAR at which CV charging can achieve the target adsorptions are subsets of the ranges of ASAR at which CC can achieve the same target adsorptions, as shown in Figure 6A and 6B. For target adsorptions with lower $\overline{c}_D$, CV charging can operate in a high ASAR range that CC charging cannot operate, because CC charging in that ASAR range requires the cell voltage to increase beyond the chosen cutoff voltage of 1.8 V. On the other hand, CC charging can operate in a low ASAR range in which CV charging fails to operate, as CV charging in that ASAR range requires an applied voltage that is too low to remove enough salt for achieving the target adsorption.

IMPLICATIONS

The performance of CC and CV charging in an MCDI process was compared systematically using the SEC^{-1} vs ASAR curves that quantify the intrinsic trade-off between energetic and kinetic efficiencies—the two most significant technical performance indicators in any desalination process. These trade-off curves are carefully established to ensure that all charging operations on a trade-off curve achieve the same target adsorption. This framework of performance evaluation can be extended to different types of comparisons. For example, we can compare two MCDI processes using different electrodes, or spacers, or ion exchange membranes; we can also compare CDI processes with flow-by and flow-through configurations, or even compare MCDI and CDI processes, as long as we can construct the SEC^{-1} vs ASAR curves for the two processes being compared, making sure they both achieve the same target adsorption.

Our analysis suggests that whether CC or CV charging is more efficient is largely dependent on the target adsorption to be achieved. There seems to be no simple rule for facile prediction of the more favorable charging mode with a given target adsorption. However, the difference in efficiency between the charging modes is always relatively small as suggested in Figure 7. Moreover, our analysis uncovers an additional aspect beyond "which is better" when comparing the CC and CV charging: there exist operating regimes, defined by both target adsorption and ASAR, in which only one of the two charging mode can achieve. All these observations suggest that there is no definitive performance advantage of one charging mode over the other. Therefore, the selection of charging mode in practice has to be guided by experimental evaluation or numerical simulation to identify the more efficient charging mode for achieving a specific target adsorption. Lastly, it should be noted that energetic and kinetic efficiencies are not the only aspects for deciding the charging mode in MCDI. The widely recognized superior controllability of effluent salinity in CC charging may also be an important advantage in engineering practice.

ASSOCIATED CONTENT

Supporting Information

The Supporting Information is available free of charge on the ACS Publications website at DOI: 10.1021/acs.est.7b06064.

Description of the dynamic ion transport model; constrains of CC and CV charging in achieving a target adsorption; figures and tables as described in the text (PDF)

AUTHOR INFORMATION

Corresponding Author

*Phone: +1 (615) 322-7226; e-mail: shihong.lin@vanderbilt.edu.

ORCID

Li Wang: 0000-0002-5542-6696

Shihong Lin: 0000-0001-9832-9127

Notes

The authors declare no competing financial interest.

ACKNOWLEDGMENTS

S. Lin acknowledges the support from Oak Ridge Associated Universities (ORAU) through the Ralph E. Powe Jr. Faculty Enhancement Award. We are also grateful to P.M. Biesheuvel for providing helpful guidance in developing and implementing the dynamic ion transport model. Last but not least, we are also thankful to the reviewers and P. M. Biesheuvel (again) for carefully reading the manuscript and providing invaluable suggestions for improvements.

REFERENCES

(1) Porada, S.; Zhao, R.; van der Wal, A.; Presser, V.; Biesheuvel, P. M. Review on the science and technology of water desalination by capacitive deionization. *Prog. Mater. Sci.* **2013**, *58* (8), 1388−1442.

(2) Zhao, R.; Porada, S.; Biesheuvel, P. M.; Van der Wal, A. Energy consumption in membrane capacitive deionization for different water recoveries and flow rates, and comparison with reverse osmosis. *Desalination* **2013**, *330*, 35−41.

(3) Anderson, M. A.; Cudero, A. L.; Palma, J. Capacitive deionization as an electrochemical means of saving energy and delivering clean water. Comparison to present desalination practices: Will it compete? *Electrochim. Acta* **2010**, *55* (12), 3845−3856.

(4) Zhao, R.; Biesheuvel, P. M.; van der Wal, A. Energy consumption and constant current operation in membrane capacitive deionization. *Energy Environ. Sci.* **2012**, *5* (11), 9520−9527.

(5) Porada, S.; Sales, B. B.; Hamelers, H. V. M; Biesheuvel, P. M. Water Desalination with Wires. *J. Phys. Chem. Lett.* **2012**, *3* (12), 1613−1618.

(6) Mossad, M.; Zhang, W.; Zou, L. Using capacitive deionisation for inland brackish groundwater desalination in a remote location. *Desalination* **2013**, *308*, 154−160.

(7) Forrestal, C.; Xu, P.; Ren, Z. Y. Sustainable desalination using a microbial capacitive desalination cell. *Energy Environ. Sci.* **2012**, *5* (5), 7161−7167.

(8) Yang, Z. Y.; Jin, L. J.; Lu, G. Q.; Xiao, Q. Q.; Zhang, Y. X.; Jing, L.; Zhang, X. X.; Yan, Y. M.; Sun, K. N. Sponge-Templated Preparation of High Surface Area Graphene with Ultrahigh Capacitive Deionization Performance. *Adv. Funct. Mater.* **2014**, *24* (25), 3917−3925.

(9) Wang, Y.; Zhang, L. W.; Wu, Y. F.; Xu, S. C.; Wang, J. X. Polypyrrole/carbon nanotube composites as cathode material for performance enhancing of capacitive deionization technology. *Desalination* **2014**, *354*, 62−67.

(10) Peng, Z.; Zhang, D. S.; Shi, L. Y.; Yan, T. T. High performance ordered mesoporous carbon/carbon nanotube composite electrodes for capacitive deionization. *J. Mater. Chem.* **2012**, *22* (14), 6603−6612.

DOI: 10.1021/acs.est.7b06064
Environ. Sci. Technol. 2018, 52, 4051−4060

(11) Wang, Z.; Yan, T. T.; Shi, L. Y.; Zhang, D. S. In Situ Expanding Pores of Dodecahedron-like Carbon Frameworks Derived from MOFs for Enhanced Capacitive Deionization. *ACS Appl. Mater. Interfaces* **2017**, *9* (17), 15068−15078.
(12) Zhao, S. S.; Yan, T. T.; Wang, H.; Zhang, J. P.; Shi, L. Y.; Zhang, D. S. Creating 3D Hierarchical Carbon Architectures with Micro-, Meso-, and Macropores via a Simple Self-Blowing Strategy for a Flow-through Deionization Capacitor. *ACS Appl. Mater. Interfaces* **2016**, *8* (28), 18027−18035.
(13) Hemmatifar, A.; Stadermann, M.; Santiago, J. G. Two-Dimensional Porous Electrode Model for Capacitive Deionization. *J. Phys. Chem. C* **2015**, *119* (44), 24681−24694.
(14) Biesheuvel, P. M.; Zhao, R.; Porada, S.; van der Wal, A. Theory of membrane capacitive deionization including the effect of the electrode pore space. *J. Colloid Interface Sci.* **2011**, *360* (1), 239−248.
(15) Rica, R. A.; Ziano, R.; Salerno, D.; Mantegazza, F.; Bazant, M. Z.; Brogioli, D. Electro-diffusion of ions in porous electrodes for capacitive extraction of renewable energy from salinity differences. *Electrochim. Acta* **2013**, *92*, 304−314.
(16) Hassanvand, A.; Chen, G. Q.; Webley, P. A.; Kentish, S. E. Improvement of MCDI operation and design through experiment and modelling: Regeneration with brine and optimum residence time. *Desalination* **2017**, *417*, 36−51.
(17) Cho, Y.; Lee, K. S.; Yang, S.; Choi, J.; Park, H. R.; Kim, D. K. A novel three-dimensional desalination system utilizing honeycomb-shaped lattice structures for flow-electrode capacitive deionization. *Energy Environ. Sci.* **2017**, *10* (8), 1746−1750.
(18) Lee, J.; Kim, S.; Yoon, J. Rocking Chair Desalination Battery Based on Prussian Blue Electrodes. *Acs Omega* **2017**, *2* (4), 1653−1659.
(19) Suss, M. E.; Baumann, T. F.; Bourcier, W. L.; Spadaccini, C. M.; Rose, K. A.; Santiago, J. G.; Stadermann, M. Capacitive desalination with flow-through electrodes. *Energy Environ. Sci.* **2012**, *5* (11), 9511−9519.
(20) Yang, S.; Choi, J.; Yeo, J. G.; Jeon, S. I.; Park, H. R.; Kim, D. K. Flow-Electrode Capacitive Deionization Using an Aqueous Electrolyte with a High Salt Concentration. *Environ. Sci. Technol.* **2016**, *50* (11), 5892−5899.
(21) Garcia-Quismondo, E.; Santos, C.; Soria, J.; Palma, J.; Anderson, M. A. New Operational Modes to Increase Energy Efficiency in Capacitive Deionization Systems. *Environ. Sci. Technol.* **2016**, *50* (11), 6053−6060.
(22) Garcia-Quismondo, E.; Gomez, R.; Vaquero, F.; Cudero, A. L.; Palma, J.; Anderson, M. New testing procedures of a capacitive deionization reactor. *Phys. Chem. Chem. Phys.* **2013**, *15* (20), 7648−7656.
(23) Gao, X.; Porada, S.; Omosebi, A.; Liu, K. L.; Biesheuvel, P. M.; Landon, J. Complementary surface charge for enhanced capacitive deionization. *Water Res.* **2016**, *92*, 275−282.
(24) Gao, X.; Omosebi, A.; Landon, J.; Liu, K. L. Surface charge enhanced carbon electrodes for stable and efficient capacitive deionization using inverted adsorption-desorption behavior. *Energy Environ. Sci.* **2015**, *8* (3), 897−909.
(25) Gao, X.; Omosebi, A.; Landon, J.; Liu, K. L. Enhanced Salt Removal in an Inverted Capacitive Deionization Cell Using Amine Modified Microporous Carbon Cathodes. *Environ. Sci. Technol.* **2015**, *49* (18), 10920−10926.
(26) Cohen, I.; Avraham, E.; Noked, M.; Soffer, A.; Aurbach, D. Enhanced Charge Efficiency in Capacitive Deionization Achieved by Surface-Treated Electrodes and by Means of a Third Electrode. *J. Phys. Chem. C* **2011**, *115* (40), 19856−19863.
(27) Zhang, Y. M.; Zou, L. D.; Wimalasiri, Y.; Lee, J. Y.; Chun, Y. Reduced graphene oxide/polyaniline conductive anion exchange membranes in capacitive deionisation process. *Electrochim. Acta* **2015**, *182*, 383−390.
(28) Choi, J. H. Comparison of constant voltage (CV) and constant current (CC) operation in the membrane capacitive deionisation process. *Desalin. Water Treat.* **2015**, *56* (4), 921−928.
(29) Kang, J.; Kim, T.; Jo, K.; Yoon, J. Comparison of salt adsorption capacity and energy consumption between constant current and constant voltage operation in capacitive deionization. *Desalination* **2014**, *352*, 52−57.
(30) Han, L. C.; Karthikeyan, K. G.; Gregory, K. B. Energy Consumption and Recovery in Capacitive Deionization Using Nanoporous Activated Carbon Electrodes. *J. Electrochem. Soc.* **2015**, *162* (12), E282−E288.
(31) Qu, Y. T.; Campbell, P. G.; Gu, L.; Knipe, J. M.; Dzenitis, E.; Santiago, J. G.; Stadermann, M. Energy consumption analysis of constant voltage and constant current operations in capacitive deionization. *Desalination* **2016**, *400*, 18−24.
(32) Lin, S. H.; Elimelech, M. Kinetics and energetics trade-off in reverse osmosis desalination with different configurations. *Desalination* **2017**, *401*, 42−52.
(33) Wang, L.; Lin, S. Intrinsic tradeoff between kinetic and energetic efficiencies in membrane capacitive deionization. *Water Res.* **2017**, *129*, 394.
(34) Wang, L.; Biesheuvel, P. M.; Lin, S. Reversible Thermodynamic Cycle Analysis for Capacitive Deionization with Modified Donnan Model. *J. Colloid Interface Sci.* **2017**, *512*, 522.
(35) Hemmatifar, A.; Palko, J. W.; Stadermann, M.; Santiago, J. G. Energy breakdown in capacitive deionization. *Water Res.* **2016**, *104*, 303−311.
(36) Zhao, R.; Satpradit, O.; Rijnaarts, H. H. M.; Biesheuvel, P. M.; van der Wal, A. Optimization of salt adsorption rate in membrane capacitive deionization. *Water Res.* **2013**, *47* (5), 1941−1952.
(37) Biesheuvel, P. M.; Hamelers, H. V. M; Suss, M. E. Theory of Water Desalination by Porous Electrodes with Immobile Chemical Charge. *Colloid Interfac Sci.* **2015**, *9*, 1−5.
(38) Tedesco, M.; Hamelers, H. V. M; Biesheuvel, P. M. Nernst-Planck transport theory for (reverse) electrodialysis: II. Effect of water transport through ion-exchange membranes. *J. Membr. Sci.* **2017**, *531*, 172−182.
(39) Qu, Y. T.; Baumann, T. F.; Santiago, J. G.; Stadermann, M. Characterization of Resistances of a Capacitive Deionization System. *Environ. Sci. Technol.* **2015**, *49* (16), 9699−9706.
(40) Dykstra, J. E.; Keesman, K. J.; Biesheuvel, P. M.; van der Wal, A. Theory of pH changes in water desalination by capacitive deionization. *Water Res.* **2017**, *119*, 178−186.
(41) Tang, W. W.; Kovalsky, P.; Cao, B. C.; He, D.; Waite, T. D. Fluoride Removal from Brackish Groundwaters by Constant Current Capacitive Deionization (CDI). *Environ. Sci. Technol.* **2016**, *50* (19), 10570−10579.
(42) He, D.; Wong, C. E.; Tang, W. W.; Kovalsky, P.; Waite, T. D. Faradaic Reactions in Water Desalination by Batch-Mode Capacitive Deionization. *Environ. Sci. Technol. Lett.* **2016**, *3* (5), 222−226.

DOI: 10.1021/acs.est.7b06064
Environ. Sci. Technol. 2018, 52, 4051−4060